University of Huddersfield Repository

Molyneux-Berry, Paul, Bevan, Adam, Zhang, S. Y and Kabra, S

Residual Stress in Wheels: Comparison of Neutron Diffraction and Ultrasonic Methods, with Trends in RCF

Original Citation

Molyneux-Berry, Paul, Bevan, Adam, Zhang, S. Y and Kabra, S (2014) Residual Stress in Wheels: Comparison of Neutron Diffraction and Ultrasonic Methods, with Trends in RCF. In: The Second International Conference on Railway Technology: Research, Development and Maintenance, 8-11 April 2014, Corsica, France.

This version is available at http://eprints.hud.ac.uk/id/eprint/22099/

Residual Stress in Wheels: Comparison of Neutron Diffraction and Ultrasonic Methods, with Trends in RCF

P.B.Molyneux-Berry[1], A.J.Bevan[1], S.Y.Zhang[2] and S.Kabra[2]
[1] Institute of Railway Research, University of Huddersfield, United Kingdom
[2] ISIS, Science & Technology Facilities Council, United Kingdom

Abstract

The critical damage mechanism on many GB passenger train wheels is Rolling Contact Fatigue (RCF) cracking in the rim. Evidence from field observations suggests that RCF damage occurs much more quickly as the wheelsets near the end of their life. Wheel manufacturing processes induce a compressive hoop stress in the wheel rim; variations in residual stress through the life of a wheel may influence the observed RCF damage rates.

This paper describes experiments to measure residual stresses in new and used wheel rims to identify whether this could be a significant factor, and compares the findings from neutron diffraction and ultrasonic birefringence methods. The scope goes beyond previous applications of neutron diffraction to railway wheels and identifies key considerations for future testing.

Assuming that the as-manufactured stress distribution was similar for all three wheels tested, it is found that the stresses are redistributed within the wheel rim during its life as material is removed and plastic flow occurs. However, the hoop stress near the running surface remains compressive and may not have a large influence on the RCF damage rates.

Keywords: railway wheel neutron diffraction residual stress.

1 Introduction

Railway wheels operate in a demanding environment with high normal contact forces and significant tangential forces. The resulting stresses often exceed the yield stress of the as-manufactured wheel material, leading to plastic flow, wear and fatigue damage. Wheelset maintenance and renewal comprises a significant portion of the whole-life cost of railway rolling stock.

In a recent survey of wheel damage on over 90% of UK passenger fleets, rolling contact fatigue (RCF) was found to be a dominant damage mechanism [1] and many

fleets have their wheels turned on a preventive distance-interval basis to control the depth of RCF cracks. The types and locations of RCF damage have been monitored and related to the operating conditions of the fleet [2].

However, the current 'state of the art' for modelling of RCF damage in railway wheels has not achieved an integrated deterministic model of wheel damage owing to the complexity of the conditions [3],[4],[5]. The authors of this paper aim to improve this modelling by researching the influences of the wheel manufacturing and maintenance processes and the operating conditions on the nature and severity of RCF crack growth.

Many factors influence the growth rate of RCF cracks in wheels, including the train type, operating and environmental conditions and the position of a wheelset in the train [1]. The experience of maintainers on several GB rolling stock fleets suggests that RCF damage occurs much more quickly as the wheelsets near the end of their life (i.e. approaching the minimum diameter before the wheelset is renewed).

Figure 1 shows examples of this trend for a regional DMU fleet monitored by the authors. Wheel diameter removed on the lathe at reprofiling is used as an indicator of crack depth. A diameter loss of ≈5mm is required to recover the wheel flange shape even when no cracks are present, but deeper cuts indicate the depth of RCF-cracked material. Wheels turned for other reasons (e.g. flats, wear, parity) are excluded. For a given mileage run since the last reprofiling, the cracks have propagated more deeply on smaller diameter wheels so the diameter loss on the lathe is greater. These statistics have been derived from the train maintainer's wheelset database, supported by the authors' observations of wheel damage and wheel turning activities.

Figure 1: Wheel diameter lost at turning (reprofiling on a lathe) to remove RCF-cracked material, for a UK multiple-unit fleet. (a) shows all wheels turned over a six-year period, (b) shows data for wheels made by one manufacturer.

The authors suggest a number of possible reasons for this effect, as listed in Table 1. This paper describes experiments to measure residual stresses in new and used wheel rims to identify whether these could be a significant factor in the observed trends in RCF damage rates.

Table 1: Possible reasons why RCF crack propagation is faster on end-of-life wheels (smaller diameter)

Possible Reason	Comment
Change in material properties (hardness, microstructure) with depth below the as-manufactured tread surface.	This has been investigated by the authors [5] and is believed to be significant.
Reduction in residual compressive stress remaining from the manufacturing process (beneficial compressive hoop stresses at the surface are lost due to plastic flow, wear and material removal at reprofiling).	Variations in residual stress have been measured [6], [7] and some models have considered their influence on RCF damage [4], which may be significant.
Increased contact stress (due to smaller wheel radius).	The change in wheel diameter is ≈6% which would increase the Hertzian contact stress by ≈2%; while this may be a contributory factor it is probably not sufficient to be the sole cause.
Higher number of stress cycles for a given wheelset mileage (due to increase in number of wheel revolutions).	The change in revolutions/mile is ≈6%; while this may be a contributory factor Figure 1 indicates that this is insufficient to be the sole cause.
Reduced wheelset rolling inertia increasing the probability of wheel spin or slide events. These cause thermal damage which can accelerate crack initiation or propagation.	Improvements in the wheel slide protection and traction control software have reduced the occurrence of these events, and they are excluded from the data presented in Figure 1. However, they may be a contributory factor on some fleets.
'Human factors' issues: in an attempt to prolong wheel life, the lathe operator may minimise the cut depth on a small wheel, and thereby not remove all previous damage.	This has been identified as a problem on some fleets, and may be relevant but is difficult to assess and quantify. Considering the experience of the staff at the depot and the detailed monitoring undertaken by the authors, this is unlikely to have a significant influence on the fleet whose trends are shown in Figure 1.

2   Influence of manufacture and running in service

Modern multiple-unit trains running in the UK are fitted with one-piece forged wheels, usually to the rim-chilled hypoeutectoid grade known as R8T or ER8T. The chemical composition and properties of the steel are tightly defined by the relevant national and international standards [8], [9].

The manufacturing process for these wheels is complex [10], and also well described in online literature [11], [12]. After rough machining, the wheel is heated to approximately 900°C (austenitisation) and the wheel rim (only) is then rapidly water quenched to 300°C. The wheel is then left to slowly air-cool. This process achieves two key goals:

- The rapid rim quenching makes the wheel rim material harder than the wheel centre, and thus more resistant to wear and crack initiation.

- The slow contraction of the web and centre during air-cooling causes compressive residual hoop stresses in the already-hardened wheel rim, thereby making it more resistant to crack propagation.

During operation, the running surface of the wheel is subjected to cyclic high contact stresses which cause plastic flow of the material within ≈1mm of the surface, and hardening through dislocation density growth to a depth of ≈6mm [5]. RCF cracks often form in these regions. Material is also lost from the running surface by wear (≈1mm per 100,000km run in the region most affected by RCF). Finally, when the wheel is reprofiled, material to a depth of ≈5mm may be turned off on the lathe. All these effects could influence the residual stress distribution within the wheel rim, both locally in the near-surface regions and at a greater depth within the wheel rim.

4 Measuring residual stresses in wheels

4.1 Selection of techniques

Many techniques are available for measuring residual stresses or strains, but not many can be effectively applied to large solid steel components such as railway wheels. The significant residual stresses in a wheel are relaxed by cutting operations, so it is usually necessary to test an entire wheel, which is typically 900mm in diameter and has a mass of 400kg. Table 2 lists some methods which can be applied to wheels in practice.

Considering these methods, it was decided to use the simple ultrasonic birefringence method on several wheels, and then to test a sub-set of these using neutron diffraction. Starting with non-destructive methods allows the possibility of subsequent destructive tests on the same samples for comparison purposes.

After completion of the ultrasonic testing, one wheel was sectioned to provide stress-free reference samples for the neutron diffraction measurements. An initial radial cut was made to evaluate the simplest of the destructive techniques, and to gain experience in EDM cutting of entire wheels for a possible future application of the contour method [13].

Table 2: Methods for measuring residual stresses or strains in railway wheels

Method	Type	Notes
Radial cut, measure closing of gap	Destructive	Defined in UK standards [9]. Simple to carry out but limited information obtained.
Strain-gauging of segment followed by progressive material removal	Destructive	Defined in EN standards [8]. More complex method but only provides a general overview of residual strains.
Hole drilling	Destructive	Near-surface: max depth similar to hole diameter, typically ≈2mm
Contour method: accurate co-ordinate measuring of a cut surface to determine which parts have bulged when stress is released	Destructive	Can provide very good stress distribution across the cut surface [13]. Relies on a very high quality smooth EDM cut which is difficult to achieve with the size and cross-section of a wheel, which also tends to close up the cut faces and trap the EDM wire.
Ultrasonic birefringence techniques [7][14]	NDT	Commercially available and portable but provides only an indirect measure of strain averaged through the wheel rim width. May be used for manufacturing quality control [9] and failure investigations.
Neutron diffraction	NDT	Can measure 3D strain field a small 'gauge volume' within the bulk of a sample several centimetres thick [6]. Limited beamtime available, few facilities can handle large/heavy samples.
Barkhausen noise techniques	NDT	Near-surface only, difficult to differentiate between stress and microstructure effects
Finite element analysis (FEA) in conjunction with another method	N/A	FEA of manufacturing processes [15],[16] can predict stress distributions, which can be compared to limited measurements from other methods described above. FEA can also be used in conjunction with sectioning methods to improve the resolution of results. However, FEA of the inhomogeneous, anisotropic, plastically flowed and cracked material near the running surface of the wheel is difficult.

4.2 Wheel samples

Four wheels were used for the tests. All wheels were manufactured to the same design by the same manufacturer, for use on the fleet of trains showing the trends illustrated in Figure 1.

One new wheel of 851mm diameter (Ø) was never fitted to an axle or used. Two mid-life wheels of Ø831mm were removed from service after 389,000 miles and had been reprofiled twice. These ran on the same bogie and had an identical history: one of these was sectioned to provide stress-free samples. One end-of-life wheel of Ø796mm was acquired after removal from service: this ran on the same train as the mid-life wheels but had been fitted earlier, running 686,000 miles and being reprofiled four times.

All three used wheels had run 132,000 miles since they were last reprofiled on the lathe. The mid-life wheels had a band of mild RCF cracking 95-105mm from the flangeback, while the end-of-life wheel had a more severe band of RCF cracks and cavities in the range 75-105mm from the flangeback, as shown in Figure 2.
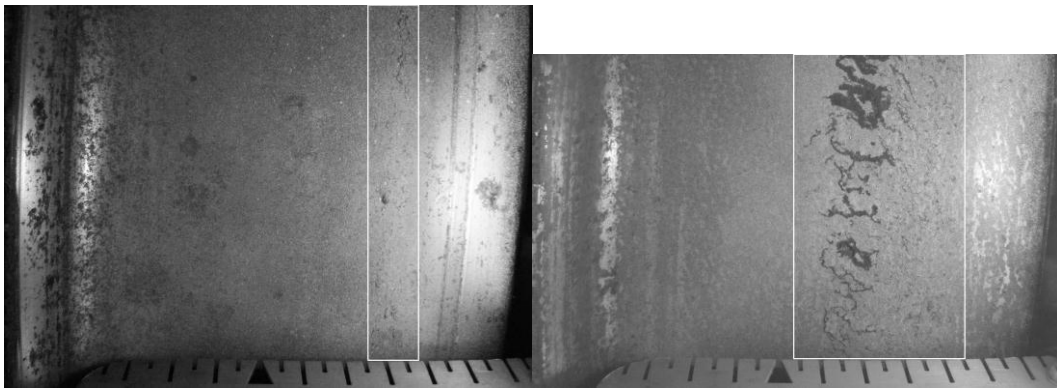

Figure 2: Photographs of wheel tread surfaces on (L) mid-life wheel, (R) end-of-life wheel, showing RCF cracking enhanced using dye penetrant. Flange to left, scale at bottom in 10mm/5mm increments: triangle indicates 70mm from flangeback.

4.3 Ultrasonic birefringence methodology

Ultrasonic residual stress measurements are based on the elastoacoustic effect: the velocity of an ultrasonic wave depends on the elastic strain in the material it is passing through. The 'Debbie' probe [14] is applied to the wheel flangeback face, and generates ultrasonic waves through the wheel rim travelling in the axial direction. It sends two waves polarised in the radial and circumferential/hoop directions, measures the wave times of flight, and calculates the acoustic birefringence from the difference in flight times. This can be related to the difference in elastic strain using the elastoacoustic constant [14]. The measured birefringence is the sum of two effects:

- Stress induced anisotropy: This has a linear relationship to the difference between the circumferential and radial strains

- Texture induced anisotropy: This is a function of the grain structure of the steel, and can therefore vary with material and radial position in the rim. It is related to the stress-free lattice parameter d_o discussed in Section 5.4.

Although the strain measured by 'Debbie' is the difference between circumferential and radial, it is usually assumed that the radial strain is small and

can be ignored, and that the circumferential strain can be related linearly to the circumferential stress. It is therefore reasonable to estimate of the circumferential stress from the stress induced anisotropy. However, to provide an effective calibration between birefringence and stress it is necessary to quantify the influence of the texture induced anisotropy. In theory, this can be done by testing a sample of near-identical wheel rim in a stress-free condition. However, achieving a stress-free wheel rim segment of sufficient size to apply the sensor without altering the microstructure of the material is not straightforward.

For comparison with the neutron diffraction measurements, it was decided not to apply any form of correction for the texture induced anisotropy to the 'Debbie' measurements. The consequences of this are discussed in Section 6.2.

The 'Debbie' measurements include a degree of spatial averaging, because the sensor is 22mm wide, and the beam crosses the full width of the wheel rim. However, it is straightforward to measure the variation in 'stress' reading as a function of radial position in the rim. The sensor was applied to the flangeback face of the wheel rim. Where there was no opposite flat face on the rim, some spurious results were identified; these were in the regions opposite the last turning groove and the tread chamfer. It is possible to adjust the sensor settings to reduce spurious echoes but they could not be eliminated completely.

5   Neutron diffraction methodology

5.1   Previous applications to railway wheels

Neutron diffraction is a non-destructive technique for accurate measurements of residual strains and stresses, and offers the capability to measure strains in a small 'gauge volume' within the bulk of a large sample [6]. Several researchers have measured residual strains in railway wheels using neutron diffraction techniques. These have focused on the stresses of newly manufactured wheels [6], [17] and the influence of running on radial strains [18], but only near the running surface of the wheel. In the existing literature there is no publication describing neutron diffraction measurements of hoop strain in wheels that have run in service, nor of wheels that have had material removed by turning.

5.2   Wheel configuration

The measurements described here were performed at the ISIS Rutherford Appleton Laboratory on the ENGIN-X instrument [19], which is one of the few facilities capable of handling such large and heavy samples. ENGIN-X is a time-of-flight facility using a spallation neutron source, so multiple diffraction peaks can be obtained simultaneously. This enables the lattice spacing to be obtained directly using a Rietveld refinement of a time-of-flight profile; this is carried out using GSAS software [20].

Collimators on the incident and detected beams allow the user to define a small 'gauge volume' for each measurement; in this case a $4 \times 4 \times 4$mm cube. Samples are

mounted on a numerically-controlled table which can be positioned so that the desired region of the sample is within the measured gauge volume. The SScanSS software [21],[22] can be used to simulate the tests, prepare numerical scripts to position the samples, and to predict the neutron beam path length through the wheel, and hence the time required to achieve a clear diffraction spectrum.

In this experiment, the wheels were mounted vertically when measuring radial and axial strains (Figure 2a) and at an elevation of 20° from the horizontal for the hoop strains (Figure 2b). Previous experiments [6] used a 60° elevation for the hoop strain measurements, favouring measurements across the tread surface at the expense of measurements through the depth of the rim.
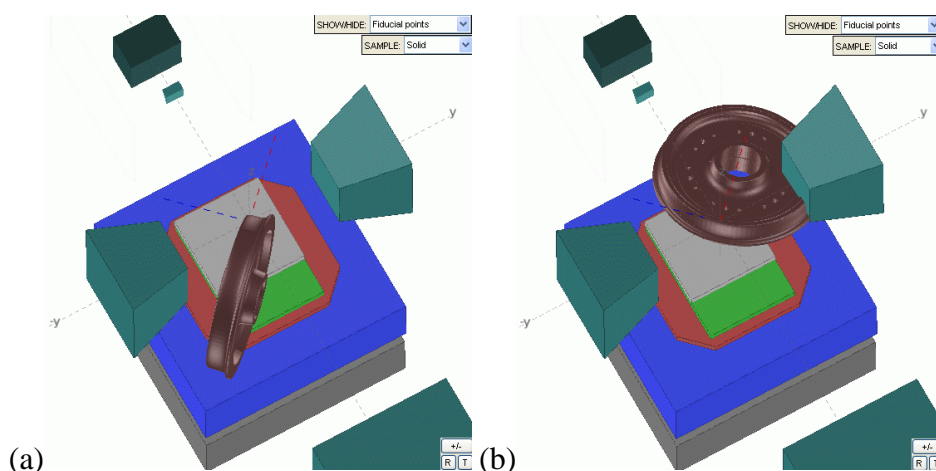

(a)   (b)

Figure 2: (a) Wheel orientation for measurement of radial and axial strains shown in SScanSS simulation. The incident beam approaches from the upper left, and measurements of neutrons reflected at 90° indicate the strain in the direction bisecting that angle. The radial strain (red dotted line) is measured in bank 1 (right) and the axial strain (blue dotted line) in bank 2 (left). (b) Wheel orientation for measurement of hoop strain. Note that this orientation (positioned at 20° from the horizontal) requires the removal of the bank 1 collimator; the hoop strain measurements are made in bank 2 (left).

5.3 Measurement points

Although neutron diffraction is one of the most penetrative non-destructive techniques for strain measurement, there are practical limitations on the regions of the wheel that can be tested. For steel samples tested on ENGIN-X, the relationship between the path length in mm and the minimum test time in minutes is as follows:

$$\text{time} = 0.2229 \times e^{(0.1146 \times \text{path length})}$$

The low rate of neutrons reaching the detector for longer path lengths mean that these measurements are more affected by 'noise' from randomly scattered neutrons. SScanSS software was used to determine the path length and therefore the minimum test time for each strain direction in each gauge volume in the wheel.

Figure 3 indicates the total test time to achieve the axial/radial and hoop strain measurements at each point in the wheels, ignoring any set-up time for the different

7

wheel orientations. If the total time to measure the 3 strain components at a single point is over 24 hours, this is shown in black and may be considered impractical. On the new and mid-life wheels, the measurable regions are limited to the flange and the field side regions near the tread (running) surface or rim face. In practice, these wheels rarely suffer any failures in the flange so the stresses in that region are of less interest.
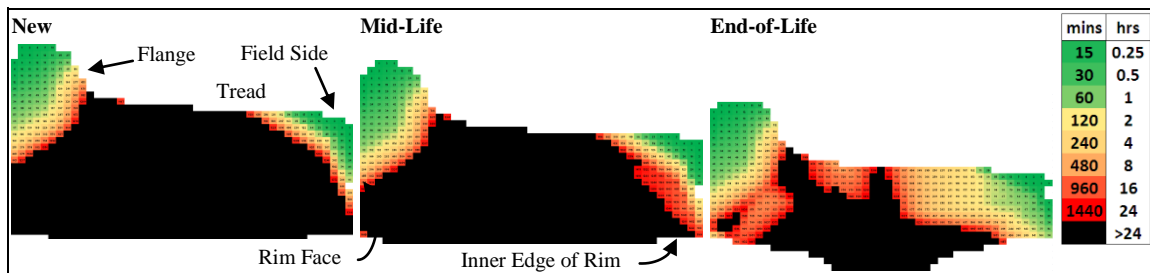

Figure 3: Time to measure all three principal strains at a location in the wheel rim, for New, Mid-life and End-of-life wheels. Regions of the wheel are annotated for reference in the subsequent description.

The end-of-life wheel presents quite a different picture to the other two, because there are plausible path lengths for hoop strain measurements with the beam entering from the inner edge of the wheel rim. Using the shallow 20° elevation enables this approach, and the path length for radial strain measurements becomes the limiting factor in many areas of the rim. Even so, the total time for strain measurements at a single point toward the centre of the wheel rim is around 8 hours, strictly limiting the number of points that can be measured in a realistic beam-time allocation of a few days.

The measurement 'gauge volumes' on each sample were selected to optimise use of the available beam-time, and measured the field side region as far as practical through the depth of the rim.

5.4 Determination of stress-free lattice parameter

The determination of residual stress from diffraction data is based on the difference between the lattice spacing in the stressed condition and the spacing in a stress-free condition. It is therefore important to know the stress-free lattice spacing (d_o) for the sample being considered [23]. Previous work by the authors has identified that the material properties within the wheel rim are anisotropic and inhomogeneous [5], with variations in ferrite fraction and plastic flow in the near-surface region.

It is plausible that the stress-free lattice spacing is influenced by these variations, so the d_o was measured in all three principal directions (radial, axial and hoop) at locations across the rim using two 'comb' samples, with comb teeth cut in the axial and radial directions to relieve the stresses in the samples. Measurements were made to coincide with the planned gauge volumes in the entire wheels, plus a coarse grid across the remainder of the wheel rim to characterise any overall trends. The comb

8

samples were cut from a wheel nearly identical to the entire mid-life wheel used in the main series of tests, and are shown in Figure 4.

Figure 4: Stress-free comb samples cut from wheel rim using EDM

The variations of d_o with depth and direction are presented in Figure 5, as a function of depth below the running surface. Each data point on this graph is the average of measurements at that depth, and the horizontal 'error' bars indicate the range of those measurements.
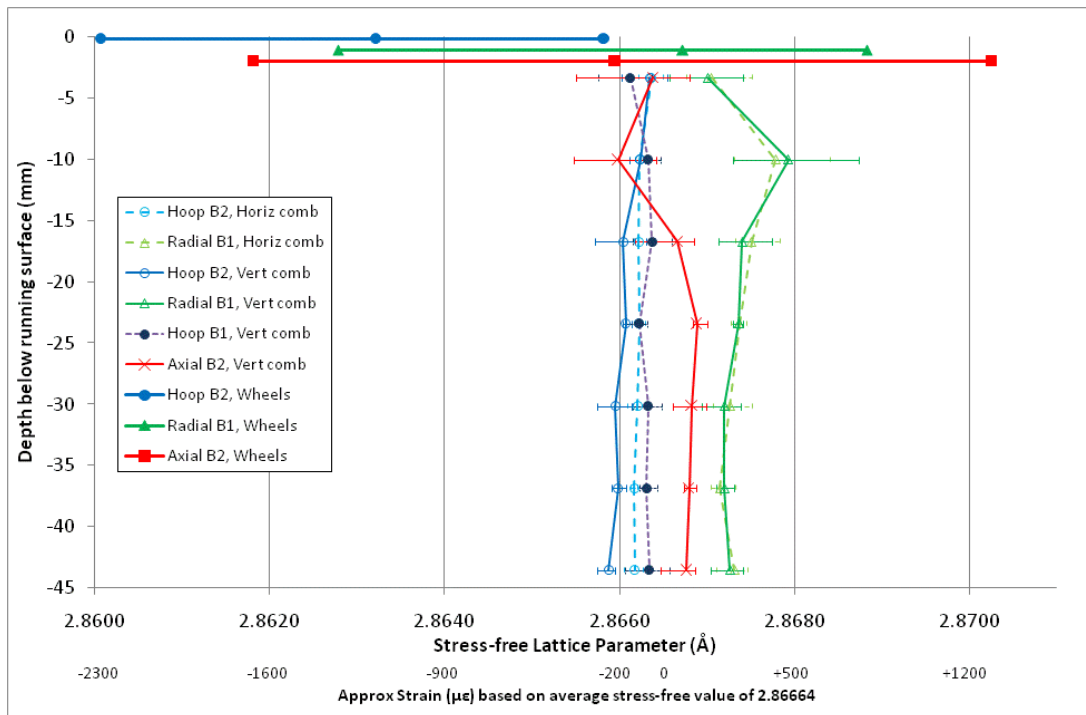

Figure 5: Variation of d_o with depth and direction

The results in the hoop direction (blue) do not vary significantly with depth. They are similar for both comb slicing directions and in both detector banks (B1, B2) suggesting that there is no great disparity of calibration between the detector banks.

Because the comb samples are so thin, it was practical to record very well-defined diffraction peak spectra, which were converted to strains using the GSAS Rietveld refinement software [20]. The fitting errors reported by the software were significantly smaller than the observed variations with location in the wheel rim.

The heavy blue bar at the top of the graph indicates the full range of hoop lattice parameter measurements in the entire wheels (as described in the following section of this paper). This is included to put the observed variations in stress-free lattice parameter into context. An approximate equivalent strain scale is included below the x-axis for information.

The axial and radial d_o measurements have a distinctly larger lattice parameter than those in the hoop direction. There are also more significant variations with depth below the running surface. In particular, the plastically flowed region on the field-side chamfer influences both the axial and radial measurements in the near-surface regions.

The heavy red and green bars at the top of the graph indicate the full range of axial and radial lattice parameter measurements in the entire wheels (as described in the following section of this paper). These put the observed variations in stress-free lattice parameter into context.

It is clear that the variations in d_o with direction and location within the sample are not insignificant when compared to the range of strains measured in the entire wheels. The extreme range of d_o measurements represents $\approx 1000\mu\varepsilon$ (microstrain), equivalent to a stress of ≈ 200 MPa. This is a useful conclusion in its own right, but leads to a dilemma regarding the selection of appropriate d_o values to use in the interpretation of the entire-wheel test results. Three options may be considered:
- Use a single average d_o value for all directions and locations (2.86664Å).
- Use a typical d_o value for each strain direction, but constant with location.
- Use the measured d_o value for the location closest to the point measured in the entire wheel sample.

The latter option was selected; it is most accurate for the mid-life wheel (near-identical to the wheel used for d_o measurements) but using this approach for the new wheel and end-of-life wheel assumes that the d_o variations in those wheels follow a similar pattern.

6 Results

6.1 Neutron diffraction results

Radial, axial and hoop strains were measured in gauge volumes distributed through the measurable regions of the field side of the rim. These gauge volumes are indicated by coloured blocks on Figure 6. Note that this figure only shows the field side of each wheel rim (the right hand side of each profile shown in Figure 3). Each coloured block indicates the strain measurement, with negative (compressive) values in blue and tensile values in yellow.

The wheel manufacturing process is designed to induce compressive hoop stress and this is the stress direction controlled by acceptance standards. Analysis of the results therefore focuses on the hoop direction. Figure 7(a) shows the variation of

hoop strain through the depth of the wheel rim. The upper point on each line is just below the tread running surface. Where more than one gauge volume was measured at a given depth (usually near the running surface) then the result shown is an average for that depth.
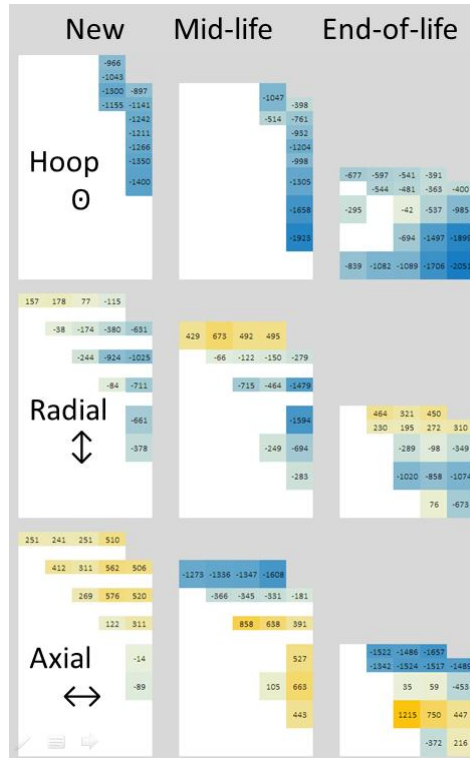

Figure 6: Strain measurements

All the hoop strains are significantly compressive and tend to increase with depth. The two used wheels show a reversal of this trend near the running surface of the wheel where significant plastic flow is present. Error magnitudes output from the Rietveld refinement software [20] are also shown; these are relatively small compared to the absolute values of strain.

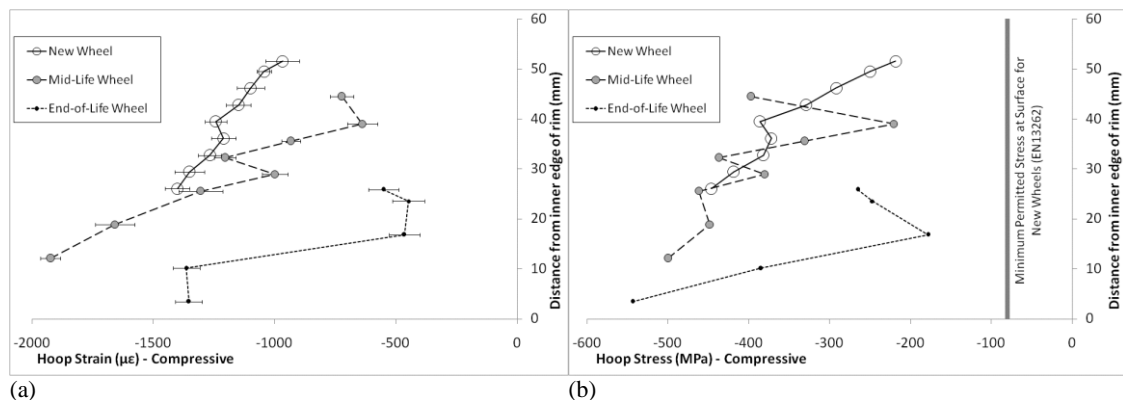(a)   (b)

Figure 7 (a) Residual hoop strain through the depth of the wheel rims, showing error magnitudes calculated by GSAS; (b) Residual hoop stress through the depth of the wheel rims, calculated from all three strain components.

11

Figure 7(b) shows the variation of hoop stress with depth; this is calculated from the radial, axial and hoop strains. The influence of the other strain components changes the trends slightly but the overall pattern remains similar. At all points measured, the hoop stresses are negative and exceed the minimum limit for hoop stress at the running surface defined in EN13262 [8].

6.2 Comparison of neutron and ultrasonic results

The two stress measurement methods do not produce results that are directly equivalent. Some care is therefore needed when comparing the results. The key differences are summarised in Table 3.

Table 3: Key differences between neutron diffraction and ultrasonic birefringence measurements and stress calculations

	Neutron	**Ultrasonic**
Location of measurement	Average of 4mm cube within wheel rim. Only practical to measure near rim face	Average across full width of wheel rim, and ≈20mm of depth
Parameter measured	Hoop, axial, radial strains independently	Difference between hoop and radial strain
Zero calibration relative to	Measured d_o varying with direction and position in rim	d_o assumed constant and value not confirmed
Hoop stress calculation	Based on 3D strain tensor	E x (hoop-radial strain)

When comparing results, it is not practical to avoid the first of the differences in Table 3. However, it is possible to process the neutron diffraction results differently to determine the influence of the other three differences. Figure 8 shows the comparison for the new wheel.
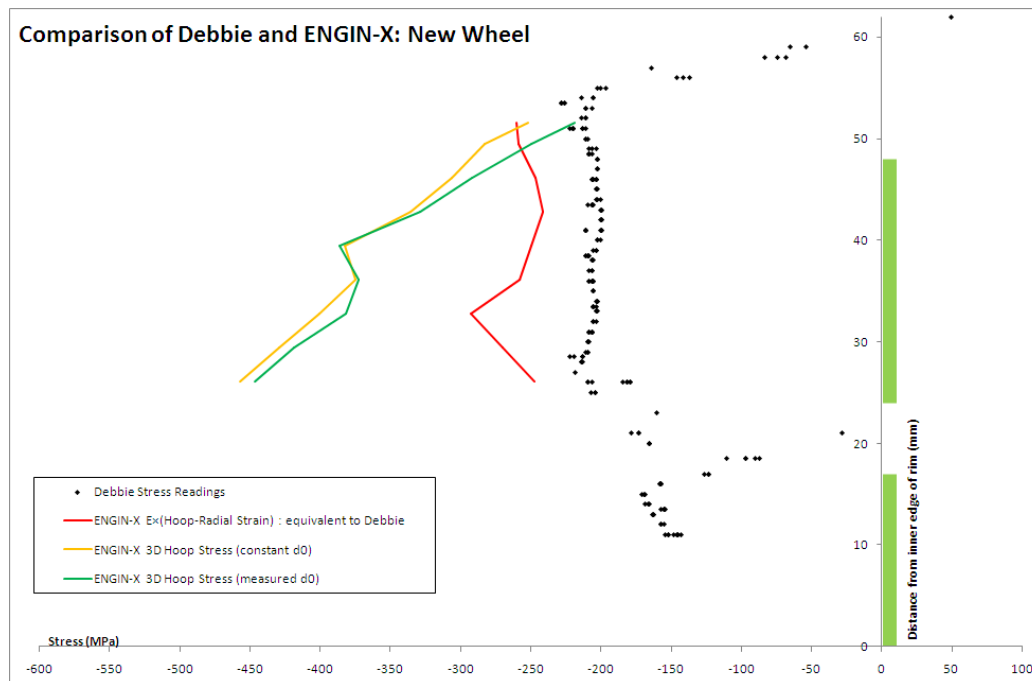
Figure 8: Comparison between neutron and ultrasonic hoop stress measurements

The green line on Figure 8 is the same as shown in Figure 7(b) and represents the hoop stress calculated from the neutron diffraction strain tensor, using the measured d_o varying with direction and position in the wheel rim. The yellow line is from the same measurements, but based on a constant d_o value; this is similar in form.

The red line is calculated from the neutron diffraction strains, but using the calculation methodology implied by the ultrasonic measurements; i.e. the difference between the hoop and radial strains, multiplied by the Young's modulus. This shows a quite different trend, but more similar to the trend in the black spots representing the 'Debbie' ultrasonic stress readings.

Assuming that the strains measured by neutron diffraction are representative of the strains across the entire width of the wheel rim, it appears that the two measuring methods give reasonably similar results. However, the simplifying assumptions inherent in the post-processing of the 'Debbie' ultrasonic measurements have a significant effect.

Figures 9 and 10 show the equivalent plots for the mid-life wheels and the end-of-life wheel, which tend to support these findings.
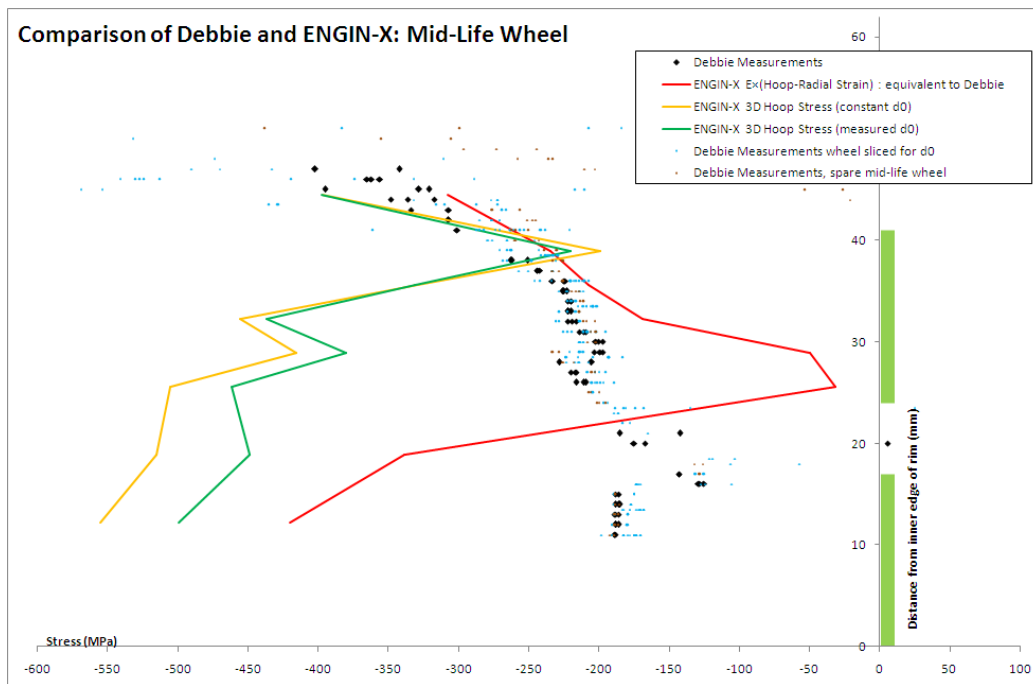

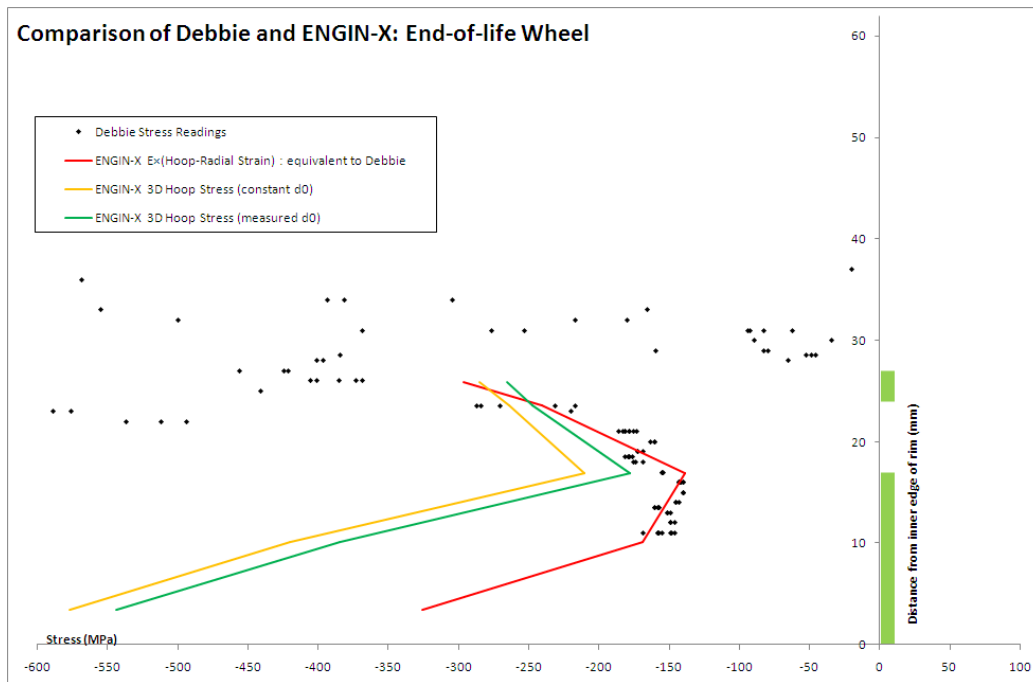Figure 9: Comparison between neutron and ultrasonic hoop stress measurements, mid-life wheels

Figure 10: Comparison between neutron and ultrasonic hoop stress measurements, end-of-life wheel

6.3 Discussion

The two measurement methods give broadly consistent results when the differences in post-processing are taken into account.

Assuming that the as-manufactured stress distribution was similar for all three wheels, the stresses are redistributed within the wheel rim during its life as material is removed and plastic flow occurs. The results suggest that the hoop stress remains significantly compressive throughout the life of the wheel rim, in excess of the minimum requirement of EN13262.

Running in service appears to increase the compressive hoop stress in the near-surface regions of the wheel.

In the field-side region of the wheel (which overhangs the wheel web), the compressive hoop stresses may be reacted by radial stresses, or by shear stresses that are not measurable using these methods.

Future work will assess the significance of axial, radial and shear stresses in the wheels. It is also hoped to use destructive methods of measuring residual stresses to provide additional results from the same wheels for comparison. This may be combined with finite element modelling.

6.4 Impact of results on wheel fatigue damage

The results suggest that the residual hoop stress in the wheel rim remains significantly compressive throughout the life of the wheel, exceeding the minimum requirements of EN13262. This suggests that hoop stresses in the rim are not a

14

significant factor in the observed increase in RCF damage rates on end-of-life wheels. Future work will consider the influence of such values of residual stress on crack growth using established fatigue models.

The neutron diffraction results also indicate significant tensile strains in the axial direction. These are in the part of the wheel where vertical split rim defects can occur, although such defects have not been observed on the design of wheel used in this experiment. Further investigation into axial tensile stresses and their influence on crack propagation would be worthwhile.

7 Conclusions

Neutron diffraction techniques can be used to measure the distribution of strains and stresses in entire railway wheels, but practical path-length limitations mean that they cannot reach the middle of the wheel rim. These measurements were therefore limited to the field side region of the wheel which may not be representative of the wheel as a whole.

Measurements of the stress-free lattice spacing d_o using comb samples indicated that this parameter is significantly anisotropic, and can also vary with position in the wheel rim.

Assuming that the as-manufactured stress distribution was similar for all three wheels, the stresses are redistributed within the wheel rim during its life as material is removed (through in-service wear and turning on a wheel lathe) and plastic flow occurs. However, the hoop stress near the running surface remains compressive, typically in the range 200MPa to 400MPa. This exceeds the minimum limit for hoop stress at the running surface defined in EN13262.

There are simplifying assumptions inherent in the post-processing of the 'Debbie' ultrasonic measurements. If the same simplified post-processing is applied to the neutron diffraction strains then the stress trends from the two methods are reasonably consistent. However, there can be significant differences between these results and the hoop stresses calculated from the full strain tensor and local d_o values.

Acknowledgements

References

[1] Bevan, A., Molyneux-Berry, P., 'Train Architecture and Operational Parameters Evaluation to Optimise Wheel Damage Control for Operators: Final Summary Report', RSSB Project T963-01, May 2013.

[2] Molyneux-Berry, P., Bevan, A., 'Wheel surface damage: relating the position and angle of forces to the observed damage patterns', IAVSD Conference, Manchester, 2011.

[3] Ekberg, A., Akesson, B., Kabo, E., 'Wheel/Rail rolling contact fatigue – probe, predict, prevent', 9th International Conference on Contact Mechanics and Wear of Rail/Wheel Systems (CM2012), Chengdu, August 27-30, 2012.

[4] Bernasconi, A., Davoli, P., Filippini, P., Foletti, S., 'An integrated approach to rolling contact sub-surface fatigue assessment of railway wheels', Wear 258 (2005) 973–980

[5] Molyneux-Berry, P., Davis, C.L., Bevan, A., 'The Influence of Wheel/Rail Contact Forces on the Material Properties of Wheels in Service', 9th International Conference on Contact Mechanics and Wear of Rail/Wheel Systems (CM2012), Chengdu, China, August 27-30, 2012.

[6] Alessandroni, M., Paradowska, A.M., Perelli Cippo, E., Senesi, R., Andreani, C., Gorini, G., Montedoro, P., Chiti, F., Sala, D., Spinelli, D., 'Investigation of Residual Stress Distribution of Wheel Rims using Neutron Diffraction', Materials Science Forum Vol 681 (2011) 522-526

[7] Mutton, P., Lynch, M.R., 'Improving the safety of railway wheels through nondestructive measurement of residual stresses'. In: Proceedings of Conference on Railway Engineering , 2004,.Darwin.

[8] 'Railway applications - Wheelsets and bogies - Wheels - Product Requirements', BS EN 13262:2004 +A2:2011

[9] 'Railway rolling stock materials - Part 3: Specification for monobloc wheels for traction and trailing stock', BS 5892-3:1992+A2:2009

[10] Diener, M., Ghidini, A., 'Reliability and safety in railway products: fracture mechanics on railway solid wheels', Lucchini RS, 2008.

[11] KLW, 'Wheels and Tyres for Railways', http://www.interpipe.biz/files/Wheels-PDF_2009.pdf

[12] 'Advanced Forging Technologies, Heat Treatment for Railway Wheels, Tyres and Rings', http://www.presstrade.com/downloads/aft/AFT_WBER_E.pdf

[13] Bouchard, J., 'Advances in the Contour Method', IMechE Conference: 'Residual Stress Engineering: Developing Control, Measurement and Characterisation Techniques', Manchester, January 2013

[14] 'Debbie: Ultrasonic measurement of hoop stress in the rim of monobloc railroad wheel, User ́s Manual', Debro UMS, Warsaw 2004

[15] Linamanaik, S.N., Chen, B.K., 'Thermo-mechanical modelling of residual stresses induced by martensitic phase transformation and cooling during quenching of railway wheels', Journal of Materials Processing Technology 211, 2011.

[16] Gordon, J., Perlman, B., 'Estimation of residual stresses in railroad commuter car wheels following manufacture', FRA report DOT/FRA/ORD-03/24, 2003.

[17] Evans, A., 'Neutrons for non-destructive residual stress characterisation for rail applications', IOM3 Conference, York, 2011

[18] Grosse M., Ottlinger, P., 'Strain measurements at railway wheels', Materials Science and Engineering A 437 (2006) 88–92

[19] Oliver, E., Santisteban, J., James, J., Daymond, M., Dann, J., 'ENGIN-X User Manual', ISIS & Open University, 16 August 2004

[20] Larson, A.C., Von Dreele, R.B., 'General Structure Analysis System (GSAS)', Los Alamos National Laboratory Report LAUR 86-748 (2004).

[21] James, J., Santisteban, J., Edwards, L., Daymond, M., 'A Virtual Laboratory for Neutron and Synchrotron Strain Scanning', Physica B, Condensed Matter (2004) 350 pp.743-746.

[22] James, J., Edwards, L., 'Application of robot kinematics methods to the simulation and control of neutron beam line positioning systems', Nuclear Instruments and Methods in Physics Research A. (2007) 571, 709-718

[23] Withers, P. J., Preuss, M., Steuwerb, A., Pangc, J. W. L., 'Methods for obtaining the strain-free lattice parameter when using diffraction to determine residual stress', Journal of Applied Crystallography, (2007). 40, 891–904

16